Hydrodynamic characterization of a shallow rectangular spouted bed using bed pressure signals and image processing methods

Jingsi Yang [a*], Ronald W. Breault [b*], Justin M. Weber [b]

[a] *Oak Ridge Institute for Science and Education, 3610 Collins Ferry Road, Morgantown, WV 26505, United States*

[b] *National Energy Technology Laboratory, U.S. Department of Energy, 3610 Collins Ferry Road, Morgantown, WV 26505, United States*

[*] Corresponding author. E-mail address: jyagn904@gmail.com (J.Yang); ronald.breault@netl.doe.gov (R. W. Breault).

ABSTRACT

To help support the design of spouted bed reactors, experiments are performed in a rectangular spouted bed to measure the peak pressure drop (ΔP_{max}), as well as the internal and external spouting velocities (U_{is} and U_{es}). Four particles spanning Geldart D and B groups are used. U_{is} and U_{es} are measured based on the bed pressure drop and bed expansion ratio, with the U_{es}/U_{is} ratio of each particle type obtained. Correlations predicting the ΔP_{max} of Geldart D and B particles are developed by reviewing published correlations and investigating the effect of the nozzle size. Good prediction is achieved with a slope of 0.997 and an adjusted R^2 of 0.998. Similarly, a correlation for U_{es} is developed by adding the effects of d_p/D_i and H_0 in the Mathur-Gisher equation. The predicted U_{es} agrees well with the experimental data, achieving a slope of 0.998 and an adjusted R^2 of 0.998.

1. INTRODUCTION

Mathur and Gishler[1] originally developed the spouted bed to compensate for the limitations of the fluidized bed in effectively handling coarse, Geldart D, particles. Inspired by unique gas-solid movement, with the high circulation rates of the particles between the core and annulus regions and the improved contact between the gas and solids caused by the formation of jet and fountain, numerous studies have revealed that the spouted-bed technique can be applied to both physical (such as drying[2], coating[3] and granulation[4]) and chemical (such as pyrolysis[5], combustion[6] and gasification[7]) processes.

The distinctive formation of a dilute central core with gas-solids concurrent flow and a dense annulus with that of countercurrent flow leads to practical benefits of spouted beds in improving the industrial efficiency, as exemplified in the following work[8-10]. By adding a jet to a bubbling fluidized bed combustor, Okasha[8] created a jetting-fountain fluidized bed (JFFB) combustor. This allowed for more effective control of the freeboard temperature and temperature profile resulting in reduced overheating. Applying a conical spouted bed reactor fitted with a draft tube and a fountain confinement device, Lopez et al.[9] improved the contact between the reacting gas and the fine Geldart B catalyst (90-150 μm), improving the biomass conversion efficiency in a biomass gasifier. Additionally, Vuthaluru and Zhang[10] demonstrated in a lab-scale spouted bed combustor that the spouted bed is exceptional at preventing agglomeration of the bed materials. In a CO_2-capture program initiated by the United States Department of Energy to capture CO_2 from existing coal-fired power plants, a spouted-bed has been proposed as a fuel reactor to overcome the accumulation of ash byproducts by elutriating ash particles from the oxygen carrier in the Chemical Looping Combustion (CLC) process. By exploiting the capability of being able to operate at very high gas velocity at the center spout/core region without slugging, aerodynamic separation can occur due to the difference in particle diameter and density. Therefore, spouted bed technology, with its unique flow characteristics, has been given a priority in reactor applications where the gas and particles contact are required to ensure a high operational efficiency.

As critical hydrodynamic characteristics, the peak pressure drop (ΔP_{max}) and the minimum spouting velocity (U_{ms}) have been predicted in different bed geometries under different operating conditions since the spouted bed was first coined by Mathur and Ghishler[1], due to their significant role in design, operation and scale-up of the spouted bed reactors.[11-14] ΔP_{max} is found to occur prior to major particle movement and is much higher than the value where the stable spouting commences.[14, 15] The extra pressure drop is believed to come from the energy required to break the interlocking of particles, allowing the internal jet to form[14]. Gelperin et al.[16] found the ΔP_{max} is two to three times higher than the pressure drop at the stable spouting in a conical bed. Asenjo et al.[17] predicated the ΔP_{max} by assuming that a laminar flow distribution exists from the injection point across the cylindrical flat-based bed. Spouting was predicated to commence when the upwards gas drag force equals the weight of solids within the enclosed volume of the gas flow. Kmieć[18] developed a correlation of the ΔP_{max} based on the empirical equation of Asenjo et al.[17] Using dimensional analysis, Ogino et al.[19] derived an equation for the ΔP_{max}. The equation indicated the ΔP_{max} is independent of the particle size and proportional to the cube root of the nozzle size and the square root of the initial static bed height. Under a certain set of conditions, particle sizes and bed dimensions, Rocha et al.[20] developed a correlation to calculate the ΔP_{max} in a pseudo two-dimensional spouted bed. It is worth noting that the ΔP_{max} correlations in the above-mentioned references [16-20] were developed with the knowledge of bed density (ρ_b) and initial static bed height (H_0), while there were other correlations that required the knowledge of the spouting pressure (ΔP_s), the pressure drop under the stable spouting.[21-23] The correlation to predict the ΔP_{max} using the ΔP_s was found earliest in the work of Mukhlenov and Gorshtein[21], which included dimensionless parameters corresponding to the geometry and particle properties. Fitting the same dimensionless moduli of the Mukhlenov-Gorshtein correlation with experimental data, Olazar et al.[22] proposed an equation for the calculation of the ΔP_{max} in conical spouted beds. Furthermore, Olazar et al.[23] proposed an empirical equation including the dimensionless parameter of nozzle inlet to bed column diameter ratio to predict ΔP_{max} in a nearly flat base spouted bed. Studying the reported ΔP_{max} correlations, some apparent contradictory results are found, for example, opposite trends have been reported between the Mukhlenov-Gorshtein correlation[21] and other references[16, 22] with respect to the effect of cone angle on ΔP_{max}. This underscores the requirement of experimental data from a wider range of bed geometries and particle properties to better understand these differences. One objective of this research is to predict ΔP_{max} from the design point of view, which includes the bed geometry and particle properties but with less parameters that rely on experimental data.

Minimum spouting velocity (U_{ms}) has been commonly defined as the superficial gas velocity at which the fountain/stable external spouting collapses in a descending gas flowrate process, which has been investigated extensively. Correlations for predicting U_{ms} have been reviewed comprehensively in previous studies[14, 24-26]. Among the previously proposed correlations, the Mathur-Gishler equation[1] has been regarded as the simplest and most widely used one, which is good to $\pm$15% for cylindrical vessels up to about 0.5 m.[14] As opposed to the descending process,[14] the U_{ms} can be determined in a gas flowrate ascending process as a transition velocity where the bed pressure drop converges to a constant value.[26, 27] Due of the pressure-drop-versus-gas-flow hysteresis phenomenon, both ΔP_{max} and U_{ms} in the gas flow ascending process are significantly higher than the values determined in the descending process because more energy is required to overcome the interlocking of particles. From a design and scaling point of view, the two hydrodynamic characteristics measured based on the ascending process are more important for the design of industrial processes, especially when designing the blowers or compressors required to supply gas for the spout during startup.[26] Specifically, this study proposes an external spouting velocity (U_{es}), defined as the superficial gas velocity where the fountain initiates in a gas flow ascending process, as identified through image processing. The relationship between the internal spouting velocity (U_{is}) and U_{es}, and the development of a U_{es} correlation will be detailed in the following sections.

As a non-intrusive method, optical techniques have gained popularity due to the continued rapid advancement of cameras, increased computational processing power, and the development of advanced image processing techniques. Applying digital image processing methods to high-speed videos for hydrodynamic characterization has been applied to a variety of gas-solid systems including circulating fluidized beds,[28, 29] fluidized beds,[30, 31] packed beds,[32, 33] and spouted beds.[34, 35] In this work, the hydrodynamic characterization of a rectangular spouted bed is based on systematic image processing methods proposed in our recent studies.[36-38] The current study aims to develop correlations requiring less secondary parameters (parameters that rely on experimental data) to predict key hydrodynamic parameters that are significant in the successful design of spouted beds. The hydrodynamic parameters requiring attention are the peak pressure drop (ΔP_{max}) and external spouting velocity (U_{es}). The accurate determination of these parameters can provide practical information for operating power and air compressor requirements and efficient evaluation in spouted bed reactors design.

2 EXPERIMENTAL APPARATUS

Experiments were conducted in a rectangular spouted bed, detailed in Figure 1(a). It consists of an acrylic rectangular column and cone, with heights of 609.6 mm and 317.5 mm, respectively. The interior cross-sectional area of the rectangular column is 30.2 mm×101.6 mm, based on which the superficial gas velocity (U_g) is calculated. The cone has an angle of 75º, the included angle is 30º. The air enters into the bed from the slotted nozzle at the bottom of cone and exits the system through two outlets at the top of the rectangular column, which are connected to a pair of filters. Two different rectangular nozzles were used in the experiments, a 19.1 mm×3.8 mm and 19.1 mm×6.6 mm, as shown in Figure 1(b). The corresponding equivalent cross-sectional area diameter (D_{eqn}) are 9.6 and 12.7 mm, which is the diameter of a circle with the same area as the rectangular nozzle. Figure 1(c) displays the arrangement of the camera and light used in this work. A Sony RX10II video camera was used to record video of the spouted bed. A Dracast LED500 light was employed to backlight the unit with a diffusional panel, providing uniform lighting to eliminating undesirable shadows and intensity gradients. Videos at 500 frames per second (fps) with a shutter time of 0.001 s and a resolution of 1920 pixel×1080 pixel were recorded and used for processing. The recorded video was post-processed frame-by-frame using the Python programing language, OpenCV[39], and Numpy[40] libraries. More information about image processing algorithms have been detailed elsewhere.[36, 37]

Geldart D particles typically spout well in both deep and shallow beds, compared to Geldart B particles that usually can only be spouted in shallow beds. [41] In the present study, four different solids, falling in Geldart D (Alumina and Nylon) and B (High density polyethylene (HDPE) and Glass beads (GB)) classifications, were used. Experiments were conducted by increasing the air flow rate. Three different initial static bed heights (H_0): 0.0762 m (3in.), 0.102 m (4 in.) and 0.127 m (5 in.), and two different nozzle sizes (D_{eqn} = 0.0096 and 0.0127 m) were varied. The beds in the present study are regarded as shallow because the particles are constrained in the cone section for all three selected H_0. Chen's study [42] in the slot-rectangular spouted beds indicated that stable spouting can be established with the particle size (d_p), nozzle length (L) and width (W) satisfying the requirements: $\sqrt{W * L}/d_p \leq 21.3$ and $L/W \leq 15$. The four particle types and two nozzle sizes used in this work satisfy the above condition. Therefore, all conditions investigated here should allow for stable spouting. A particle size and shape analyzer, Sympatec QICPIC, was used to determine the particle properties (as listed in Table 1). The air flow rate was controlled and measured using an Alicat mass flow controller with a range of 0–0.025 m^3/s. The bed pressure drop was measured by using two Setra model 239 differential pressure transducers. The pressure transducers were sampled at a frequency of 100 Hz for 120 seconds. Staticide Concentrate (#3000G, ACL Inc.) was mixed with water and placed in a bubbler. A secondary stream of air was bubble through the Staticide-water mixture and injected through a separate inlet with a flow rate of 2.5×10^{-5} m^3/s for 45 - 75 s. The Staticide and humidity significantly reduce the static electricity in the bed. This secondary flow rate was turned off during data collection (pressures and high-speed video).

3. RESULTS AND DISCUSSION

3.1 Determination of the internal spouting velocity (U_{is}) and the external spouting velocity (U_{es})

With the ascending air flow rate, the bed evolves from a fixed bed to an internal spouting flow pattern, where an air cavity is expanded into a jet. By further increasing of the air flow rate, an external spouting flow pattern can be achieved, where the internal spout reaches the bed surface and forms a fountain. Table 2 schematically illustrates the above-described flow regime evolution process. The representative regime evolutions of the four particle types under different H_0 and D_{eqn} are also shown in Table 2. In the present study, the internal spouting velocity (U_{is}), defined as the superficial gas velocity at which the internal spout originates, is determined from the bed pressure drop profile. While the external spouting velocity (U_{es}), is defined as the superficial gas velocity at which the internal spout breaks through the bed surface, is determined through the bed expansion ratio profile. The flow chart in Figure 2 illustrates the complete processing structure. The bed pressure drop profiles are plotted using the pressure signals, while the bed expansion profiles using the image processing data.

Figure 3 represents the typical bed pressure drop and bed height profiles with corresponding standard deviations of the measurement under each operating condition. Both the bed pressure drop and the bed height increases with increasing U_g, reaching a peak value before decreasing with further increase in U_g. The peak pressure drop occurs when the weight of bed material is supported and the interlocking of the particles above the internal jet is “broken up” by the gas. The maximum bed height is reached right before external spouting. Further increasing U_g decreases the bed height because the gas ejects more solids above the bed surface. Figure 3 shows a higher standard deviation in the external spouting regime (i.e. $U_g > 1.11$ m/s) for both the bed pressure and bed height. The variations of bed pressure drop with U_g for the four different kinds of particles are shown in Figure 4. Like what is shown in Figure 3, the pressure drop across the bed increases with increasing U_g until a peak value is reached, then decreases. The pressure profiles for all three bed heights and two nozzle diameters exhibit a similar parabolic trend. Further increasing U_g leads to the end of parabolic trend and the pressure drop converges to an approximately constant value. The higher H_0 results in higher overall bed pressure drop and a higher peak value. The bed expansion ratio (H/H_0) is calculated by normalizing the measured bed height with the static bed height (H_0). The profiles of H/H_0 with U_g under different H_0 for the four particles are shown in Figure 5. The profiles reflect that bed height increases to a maximum value and then decreases with the increasing U_g at the onset of the external spouting (i.e. the fountain formation). Once the external spouting is reached, the bed height decreases due to more solids being ejected above the bed surface with increasing gas flow rate. The maximum bed expansion ratio is the same and independent of H_0 for the used bed materials under the current bed configuration. This indicates that the bed expands the same ratio and does not depend on the initial static bed height. For the Geldart B particles (GB and HDPE), they reach the same value of 1.13. This may relate closely to the smaller ratio of the particle to nozzle size (i.e. $d_p/D_i \in (0.05, 0.1)$ for Geldart B particles in the present study) and the periodic bubble formation during the internal spouting regime (the minimum bubbling velocity, which is approximately the minimum fluidization velocity, i.e. 0.246 m/s for GB and 0.174 m/s for HDPE). The movement of the rising bubble from the bed bottom to the top significantly breaks up the interlocking of the particles, which is exacerbated with higher static bed heights, leading to a similar effect of H_0 on the bed expansion ratio compared to the Geldart D particles.

With the profiles of pressure drop and bed expansion ratio as a function of ascending U_g, the internal and external spouting velocities (U_{is} and U_{es}) can represent the superficial gas velocities where the internal cavity initiates and where the fountain forms. As shown in Figure 6, U_{is} is the intersection point between the linear fits of the pressure drop decreasing section and the plateau section of the bed pressure drop curve, while U_{es} is the intersection point between the linear fits of bed expansion ratio increasing and decreasing sections. U_{is} and U_{es} can be regarded as the critical velocities for the flow regime discrimination. The determination of U_{is} and U_{es} are based on the B-spline fit of the pressure drop and bed expansion ratio profiles, which were measured using discrete experimental points in the gas flow rate ascending process. Table 3 shows the determined U_{is} and U_{es} of the four types of particles under the present operating conditions. It shows that both U_{is} and U_{es} increase with H_0. With U_{is} and U_{es}, different flow regimes can be quantitively identified including, fixed bed, internal spouting and external spouting, as indicated in Figure 6.

Considering that U_{is} is determined from pressure transducer signals while U_{es} relies on image processing methods and more complex data interpretation applying complicated programming and analysis, finding a relationship between U_{is} and U_{es} provides a valuable tool for designing spouted beds. Figure 7 plots a linear correlation between U_{is} and U_{es} for the four particle types under the present operating conditions. With adjusted R square larger than 0.99, the ratio of the U_{es} to U_{is} for the four particle types are 2.07 (Nylon), 1.67 (Alumina), 1.67 (Glass beads), and 1.35 (HDPE) respectively. These values seem to imply that the U_{es}/U_{is} ratio of Geldart D particles is larger than particles of Geldart B. Note that the ratio of particle to nozzle size (d_p/D_i) for Geldart D and B particles in the present study are in the ranges of (0.1, 0.3) and (0.05, 0.1), respectively. However, considering the bed geometry of rectangular column with a rectangular nozzle and the particle properties, it is believed that more Geldart D and B particles are needed to provide enough U_{es}/U_{is} measurements before more comprehensible conclusions can be established.

3.2 Peak pressure drop

The peak pressure drop (ΔP_{max}) was determined from the typical plot of the bed pressure drop (ΔP) versus the superficial gas velocity (U_g) in a gas flow ascending process, where ΔP increases to a maximum value and then decreases with further increases in U_g, as shown in Figures 3-4. ΔP_{max} has been found higher than the pressure drop of the fully suspended bed due to the contribution of the extra pressure drop required to break up the interlocked solids above the internal jet. Figure 8 shows the effect of nozzle size on ΔP_{max} under the same H_0 for the four particle types. There is a difference in ΔP_{max} between the two nozzle sizes. This difference is larger for the Geldart B particles, compared to the Geldart D particles. This may be caused by the larger volume (i.e. more particles) above the internal jet being accelerated by the gas of the larger nozzle before external spouting, when the bed is not entirely suspended and there is less particle circulation. The lower ratio of particle size to nozzle size (d_p/D_i) and larger specific area lead to the increased effect of H_0 on the ΔP_{max} of the Geldart B than the Group D particles. The variation of ΔP_{max} with H_0 for different particle types under the same nozzle size (D_{eqn}) is illustrated in Figure 9. With the same H_0 and D_{eqn}, the order of the ΔP_{max} of the four types of particles from high to low is Alumina (ρ_p = 3150 kg/m^3), GB (ρ_p = 2300 kg/m^3), Nylon (ρ_p = 1130 kg/m^3) and HDPE (ρ_p = 860 kg/m^3), which suggests that ΔP_{max} is closely related to the particle density when the same volume of particles above the internal jet is accelerated for the same D_{eqn}. The higher particle density results in a higher weight of a particle, which needs a higher drag force to balance. Moreover, for the same particle, the increase of H_0 causes the increase of the accelerated particles' weight and the gas drag force correspondingly, which results in the ΔP_{max} increasing, as also shown in Figure 9.

Given its practical benefits to the reactor design as mentioned in the introduction section, the experimental measurements of ΔP_{max} were compared to the correlations reported in the literature.[16-23, 26] Major correlations cited in the present study are listed in Table 4. Most of the published correlations were developed based on experimental data collected in conical-cylindrical systems using Geldart D particles. This work attempts to extend these correlations to predict rectangular spouted beds using both Geldart D and B particles. Table 4 also compares the correlations using the present experimental ΔP_{max} values. Both parameters (slope and R^2) can be used to evaluate the ability of the model to predict the experimental data. The closer the slope and R^2 to 1, the better the predication. The values for the slope and R^2 of the comparisons indicate that the correlation of Ogino et al.[19] best predicts the experimental data compared to the other correlations, with a slope of 0.76 and an R^2 of 0.99. The correlation developed by Monazam et al.[26] based on a spouted-fluid bed does not predict the experimental data well, with a slope of 7.01. This is more likely due to the involvement of the annular fluidization. Figure 10 exhibits the comparison of some selected correlations with a slope < 3. Based on the correlation comparison and the above discussion of the effect of d_p/D_i on ΔP_{max} in the current bed geometry, the following relationship, based on a series of nondimensionalized parameters, is proposed:

$$\frac{\Delta P_{max}}{\rho_b g H_0} = a\left(\frac{H_0}{D_c}\right)^b\left(\frac{D_i}{D_c}\right)^c\left(\frac{d_p}{D_i}\right)^d \qquad (1)$$

The coefficients a-d in Eq. (1) are fit using nonlinear regression to the present experimental data. D_c and D_i are the equivalent cross-sectional area diameter of the rectangular column and nozzle, respectively; H_0 is the initial static bed height; ρ_b is the bulk density. Considering the corresponding range of d_p/D_i for Geldart D and B particles in the present work, the following expressions are obtained to predict the ΔP_{max} according to the particle classification:

$$\frac{\Delta P_{max}}{\rho_b g H_0} = 1.685 \left(\frac{H_0}{D_c}\right)^{0.325} \left(\frac{D_i}{D_c}\right)^{0.187} \left(\frac{d_p}{D_i}\right)^{0.116} \qquad \left(0.1 < \frac{d_p}{D_i} < 0.3, \text{Geldart D}\right) \quad (2)$$

$$\frac{\Delta P_{max}}{\rho_b g H_0} = 0.003 \left(\frac{H_0}{D_c}\right)^{-0.0324} \left(\frac{D_i}{D_c}\right)^{-1.204} \left(\frac{d_p}{D_i}\right)^{-1.380} \qquad \left(0.05 < \frac{d_p}{D_i} < 0.1, \text{Geldart B}\right) \quad (3)$$

Applying the method introduced by Johnson and Leone[43], a comparison of measured and calculated ΔP_{max} from Eqs. (2) and (3) is shown in Figure 11. The slope of 0.997, an adjusted R^2 of 0.998, and all samples falling within the 95% confidence interval demonstrates good agreement between the experimental and predicted values of ΔP_{max}. It is difficult to compare the experimental data of other research works with the calculated values using Eqs. (2) and (3) due to the lack of data provided in different studies. The application of the equivalent cross-sectional area diameters of D_i and D_c in the equations extends the possible utilization of this correlation to conical-cylindrical spouted beds.

3.3 External Spouting Velocity

In the present work, the external spouting velocity (U_{es}) is defined as the superficial gas velocity when the fountain forms in a gas flow rate ascending process. This is determined from the bed expansion ratio profile. It is different from the conventional minimum spouting velocity (U_{ms}) determined from the pressure drop profile in a descending gas flow rate process where the stable external spouting collapses. Correlations developed to predict the U_{ms} in spouted beds have been reviewed by previous researchers.[14, 24-26] Since Mathur and Gishler[1] originally published the spouted bed technique with the empirical correlation to predict the U_{ms} (as written in Eq. 4), most of the following correlations in different bed geometries and operating conditions were developed based on modification of the Mathur-Gishler equation.

$$U_{ms} = \left(\frac{d_p}{D_c}\right)\left(\frac{D_i}{D_c}\right)^{1/3}\sqrt{\frac{2gH_0(\rho_p-\rho_g)}{\rho_g}} \tag{4}$$

Eq. (4) not only shows the unit balance, but also gives the best agreement with published laboratory experiments and has been used most widely.[14] Considering the definition and particularity of the U_{es} in the present study, the development of the correlation to predict the U_{es} starts from the comparison of the Eq. (4) using the present experimental data. The results shown in Figure 12 indicates that the linear fit between the calculated ($U_{es,cal}$) and experimental ($U_{es,exp}$) values is reasonable with a R^2 of 0.99 for both Geldart D and B particles. However, there is a better agreement between $U_{es,cal}$ and $U_{es,exp}$ for Geldart B particles (slope = 1.03) than that of Geldart D particles (slope = 0.74). This suggests that the correlations of U_{es} should be split between Geldart D and B particles, since there exists significantly different particle properties and consequently, flow behavior, between the two categories.

Based on the results of Table 3 discussed in Section 3.1, that the U_{es} increases with the H_0, and the effect of particle properties and bed geometry, a correlation is proposed in based on the Eq. (4):

$$U_{es} = a\left(\frac{d_p}{D_i}\right)^b\left(\frac{D_i}{D_c}\right)^c\left(\frac{H_0}{D_c}\right)^d\sqrt{\frac{2gH_0(\rho_p-\rho_g)}{\rho_g}} \tag{5}$$

Using nonlinear regression, the coefficients a-d in Eq. (5) are fit to the data in the current study according to the ranges of d_p/D_i for both Geldart D and B solids:

$$U_{es} = 1.80\left(\frac{d_p}{D_i}\right)^{1.119}\left(\frac{D_i}{D_c}\right)^{1.467}\left(\frac{H_0}{D_c}\right)^{0.237}\sqrt{\frac{2gH_0(\rho_p-\rho_g)}{\rho_g}} \qquad \left(0.1 < \frac{d_p}{D_i} < 0.3, \text{Geldart D}\right) \tag{6}$$

$$U_{es} = 0.0121\left(\frac{d_p}{D_i}\right)^{-0.0353}\left(\frac{D_i}{D_c}\right)^{0.423}\left(\frac{H_0}{D_c}\right)^{0.0424}\sqrt{\frac{2gH_0(\rho_p-\rho_g)}{\rho_g}} \qquad \left(0.05 < \frac{d_p}{D_i} < 0.1, \text{Geldart B}\right) \tag{7}$$

Figure 13 illustrates the comparison between the experimental and predicted U_{es} using Eqs. (6) and (7) with the method introduced by Johnson and Leone[43]. A good agreement is achieved with an adjusted R^2 of 0.998, a slope of 0.998, and all samples falling in the 95% confidence interval.

Due to the difference between the definition and determination of the U_{es} in this study and U_{ms} in other works, the comparison of experimental results of other studies with the calculated values using Eqs. (6) and (7) are not applicable. However, like Eqs. (2) and (3), the utilization of equivalent cross-sectional diameters (D_i and D_c) allows for the possible extension of Eqs. (6) and (7) to conical-cylindrical spouted beds.

4. CONCLUSIONS

The present study provides the hydrodynamic characterization of a rectangular spouted bed (30.2 mm × 101.6 mm) based on the analysis of pressure drop and processing of digital images extracted from the high-speed video. The experiments were conducted in an ascending process of the gas flow rate in order to yield the critical hydrodynamic information such as the peak pressure drop (ΔP_{max}) and external spouting velocity (U_{es}), which can be used in the practical design of spouted beds. Four different kinds of solids were used as bed materials, spanning both Geldart D (Nylon and Alumina) and B (Glass beads and HDPE) groups.

The internal spouting velocity (U_{is}) was measured based on the bed pressure drop while the external spouting velocity (U_{es}) was measured based on the bed expansion ratio profiles. These two critical velocities allow for quantitative demarcations of the different flow regimes including: fixed bed, internal spouting and external spouting. The ratio of U_{es}/U_{is} for the four particle types have been obtained. However, sufficient U_{es}/U_{is} values from more Geldart D and B solids are required for more comprehensible conclusions to be established.

Correlations to predict ΔP_{max} for Geldart D and B solids were constructed by reviewing previous developed correlations available in the literature as well as incorporating the effect of the nozzle size. A good agreement between the experimental and the predicated values was achieved with a slope of 0.997, an adjusted R^2 of 0.998, and all samples falling in the 95% confidence interval.

A correlation for U_{es}, whose definition and determination is different from the conventional minimum spouting velocity (U_{ms}), was also developed based on the Mathur-Gisher equation with the effects of d_p/D_i and H_0 considered. This correlation captures the experimental fact that the U_{es} increases with the increase of H_0 and the different hydrodynamic behavior and particle properties between Geldart D and B particles. The calculated U_{es} from the developed equations agrees well with the experimental data with a slope of 0.998, an adjusted R^2 of 0.998, and all samples falling in the 95% confidence interval. Furthermore, in both developed correlations for ΔP_{max} and U_{es}, the use of the equivalent cross-sectional area diameters (D_i and D_c) allows the use of the correlations in both conical-rectangular spouted beds as well as conical-cylindrical spouted beds.

NOMENCLATURE

Ar Archimedes number, -

D_c Diameter of the cylindrical column of the spouted bed, m

D_{eqn} Equivalent cross-sectional area diameter to represent the two nozzles used in the present study, m

D_i Equivalent cross-sectional area diameter of the nozzle inlet used in the correlations, m

d_p Particle diameter (Sauter mean diameter in current research), m

g Gravity constant, m/s^2

H_0 Initial static bed height, m

U_{es} External spouting velocity, m/s

$U_{es,exp}$ Experimental value of the present external spouting velocity, m/s

$U_{es,cal}$ Calculated value of the external spouting velocity using Eqs. (6) and (7), m/s

U_g Superficial gas velocity, m/s

U_{is} Internal spouting velocity, m/s

U_m Velocity at maximum pressure drop of the spout, m/s

U_{ms} Minimum spouting velocity, m/s

Greek Letters

θ Included angle of the cone, rad

ρ_b Bulk density of the bed, kg/m^3

ρ_g Gas density, kg/m^3

ρ_p Particle density, kg/m^3

ϕ Particle sphericity, -

ΔP_M Maximum pressure drop in the references, Pa or KPa

ΔP_{max} Peak pressure drop in the present study, KPa

ΔP_s Pressure drop in the stable spouting regime, Pa

ACKNOWLEDGEMENTS

The authors acknowledge the Department of Energy for funding the research through the office of Fossil Energy Commercialization Technology Fund and the Advanced Gasification Program. Additionally, this research was supported in part by an appointment to the National Energy Technology Laboratory Research Participation Program, sponsored by the U.S. Department of Energy and administered by the Oak Ridge Institute for Science and Education.

REFERENCES

(1) Mathur, K. B.; Gishler, P. E. A technique for contacting gases with coarse solid particles. *AIChE J.* 1955, 1, 157.

(2) Benelli, L.; Souza, C. R. F.; Oliveira, W. P. Spouted bed performance on drying of an aromatic plant extract. *Powder Technol.* 2013, 239, 59.

(3) Martins, G. Z.; Souza, C. R. F.; Shankar, T. J.; Oliveira, W. P. Effect of process variables on fluid dynamics and adhesion efficiency during spouted bed coating of hard gelatin capsules. *Chem. Eng. Process: Process Intensif.* 2008, 47, 2238.

(4) Borini, G. B.; Andrade, T. C.; Freitas, L. A. P. Hot melt granulation of coarse pharmaceutical powders in a spouted bed. *Powder Technol.* 2009, 189, 520.

(5) Amutio, M.; Lopez, G.; Artetxe, M.; Elordi, G.; Olazar, M.; Bilbao. J. Influence of temperature on biomass pyrolysis in a conical spouted bed reactor. *Resour. Conserv. Recycl.* 2012, 59, 23.

(6) Konduri, R. K.; Altwicker, E. R.; Morgan III, M. H. Design and scale-up of a spouted-bed combustor. *Chem. Eng. Sci.* 1999, 54, 185.

(7) Bernocco, D.; Bosio, B.; Arato, E. Feasibility study of a spouted bed gasification plant. *Chem. Eng. Res. Des.* 2013, 91, 843.

(8) Okasha, F. M. Short overview on the jetting-fountain fluidized bed (JFFB) combustor. *Renew. Sust. Energ. Rev.* 2016, 55, 674.

(9) Lopez, G.; Cortazar, M.; Alvarez, J.; Amutio, M.; Bilbao, J.; Olazar, M. Assessment of a conical spouted with an enhanced fountain bed for biomass gasification. *Fuel.* 2017, 203, 825.

(10) Vuthaluru, H. B.; Zhang, D. K. Effect of coal blending on particle agglomeration and defluidisation during spouted-bed combustion of low-rank coals. *Fuel Process. Technol.* 2001, 70, 41.

(11) Olazar, M.; San Jose´, M. J.; Alvarez, S.; Morales, A.; Bilbao, J. Design of conical spouted beds for the handling of low-density solids. *Ind. Eng. Chem. Res.* 2004, 43, 655.

(12) Costa, M. A.; Taranto, O. P. Scale-up and spouting of two-dimensional beds. *Can. J. Chem. Eng.* 2003, 81, 264.

(13) Olazar, M.; San Jose´, M. J.; Aguayo, A. T.; Arandes, J. M.; Bilbao, J. Stable operation conditions for gas-solid contact regimes in conical spouted beds. *Ind. Eng. Chem. Res.* 1992, 31, 1784.

(14) Epstein, N.; Grace, J. R. *Spouted and spout-fluid beds: fundamentals and applications*. Cambridge: Cambridge University Press, 2011.

(15) McNab, G. S.; Bridgwater, J. Spout formation and collapse in rough and smooth walled beds. In: Grace, J. R.; Matsen, J. M. *Fluidization*. New York: Plenum Press, 1980, 271.

(16) Gelperin, N. I.; Aynshteyn, V. G.; Gelperin, E. N.; Lvova, S. D. Hydrodynamic characteristics of pseudo-liquefaction of granular materials in conical and conico-cylindrical equipment. *Khim. Tekhnol. Topliv Masel.* 1960, 5, 51.

(17) Asenjo, J. A.; Muňoz, R.; Pyle, D. L. On the transition from a fixed to a spouted bed, *Chem. Eng. Sci.* 1977, 32, 109.

(18) Kmieć, A. Hydrodynamics of flows and heat transfer in spouted beds. *Chem. Eng. J.* 1980, 19, 189.

(19) Ogino, F.; Zhang, L.; Maehashi, Y. Minimum rate of spouting and peak pressure-drop in a spouted bed. *Int. Chem. Eng.* 1993, 33, 265.

(20) Rocha, S. C. S.; Taranto, O. P.; Ayub, G. E. Aerodynamics and heat transfer during coating of tablets in two-dimensional spouted bed. *Can. J. Chem. Eng.* 1990, 70, 308.

(21) Mukhlenov, I. P.; Gelperin, A. E. Investigation of a spouted bed. *Khim. Prom.* 1965, 41, 443.

(22) Olazar, M.; San Jose´, M. J.; Aguayo, A. T.; Arandes, J. M.; Bilbao, J. Pressure drop in conical spouted beds. *Chem. Eng. J.* 1993, 51, 53.

(23) Olazar, M.; San Jose´, M. J.; Aguayo, A. T.; Arandes, J. M.; Bilbao, J. Hydrodynamics of nearly flat base spouted beds. *Chem. Eng. J.* 1994, 55, 27.

(24) Bi, H. T.; Macchi, A.; Chaouki, J.; Legros, R. Minimum spouting velocity of conical spouted beds. *Can. J. Chem. Eng.* 1997, 75, 460.

(25) Zhou, J. *Characterizing and Modeling the Hydrodynamics of Shallow Spouted Beds*. PhD Thesis University of Tennessee, Knoxville, TN, 2008.

(26) Monazam, E. R.; Breault, R. W.; Weber, J.; Layfield, K.; Minimum spouting velocity of flat-base spouted fluid bed. *Particuology.* 2018, 36, 27.

(27) Zhong, W.; Li, Q.; Zhang, M.; Jin, B.; Xiao, R.; Huang, Y. Spout characteristics of a cylindrical spout-fluid bed with elevated pressure. *Chem. Eng. J.* 2008, 139, 42.

(28) Yang, J.; Zhu, J. X. A novel method based on image processing to visualize clusters in a rectangular circulating fluidized bed riser. *Powder Technol.* 2014, 254, 407.

(29) Yang, J.; Zhu, J. X. Visualization of solids phase separation in a rectangular CFB riser using a novel image calibration method. *Powder Technol.* 2015, 273, 76.

(30) Busciglio, A.; Vella, G.; Micale, G.; Rizzuti, L. Analysis of the bubbling behaviour of 2D gas solid fluidized beds: Part I. Digital image analysis technique. *Chem. Eng. J.* 2008, 140, 398.

(31) Laverman, J. A.; Roghair, I.; van Sint Annaland, M.; Kuipers, H. Investigation into the hydrodynamics of gas–solid fluidized beds using particle image velocimetry coupled with digital image analysis. *Can. J. Chem. Eng.* 2008, 86, 523.

(32) Köhl, M. H.; Lu, G.; Third, J. R.; Häberlin, M.; Kasper, L.; Prüssmann, K. P.; Müller, C. R. Magnetic resonance imaging (MRI) study of jet formation in packed beds. *Chem. Eng. Sci.* 2013, 97, 406.

(33) Köhl, M. H.; Lu, G.; Third, J. R.; Prüssmann, K. P.; Müller, C. R. Magnetic resonance imaging (MRI) of jet height hysteresis in packed beds. *Chem. Eng. Sci.* 2014, 109, 276.

(34) Kiani, M.; Rahimi, M. R.; Hosseini, S. H.; Ahmadi, G. Mixing and segregation of solid particles in a conical spouted bed: Effect of particle size and density. *Particuology*. 2017, 32, 132.

(35) Zhang, Y.; Zhong, W.; Rui, X.; Jin, B.; Liu, H. Evaluation of mixing and mixing rate in a multiple spouted bed by image processing technique. *Int. J. Chem. Reac. Eng*. 2017, 15, 103.

(36) Yang, J.; Breault, R. W.; Weber, J. M.; Rowan, S. L. Determination of flow patterns by a novel image analysis technique in a rectangular spouted bed. *Powder Technol*. 2018, 334, 151.

(37) Yang, J.; Breault, R. W.; Rowan, S. L. Applying image processing methods to study hydrodynamic characteristics in a rectangular spouted bed. *Chem. Eng. Sci*. 2018, 188, 238.

(38) Yang, J.; Breault, R. W.; Rowan, S. L. Experimental investigation of fountain height in a shallow rectangular spouted bed using digital image analysis. *Chem. Eng. J*. 2020, 380, 122467.

(39) Bradski, G. *The OpenCV library*. Dr. Dobb's Journal of Software Tools, 2000.

(40) Oliphant, T. E. *A guide to NumPy*. Trelgol Publishing, USA, 2006.

(41) Geldart, D. *Characterization of fluidized powders, in: D. Geldart (Ed.), Gas Fluidization Technology*, John Wiley & Sons Ltd., UK, 1986, 39.

(42) Chen, Z. Hydrodynamics stability and scale-up of slot-rectangular spouted beds, *PhD thesis University of British Columbia*, Vancouver, BC, 2008.

(43) Johnson, N. L.; Leone, F. C. Statistics and Experimental Design in Engineering and the Physical Sciences, *John Wiley & Sons Ltd.*, USA, 1977, 218.

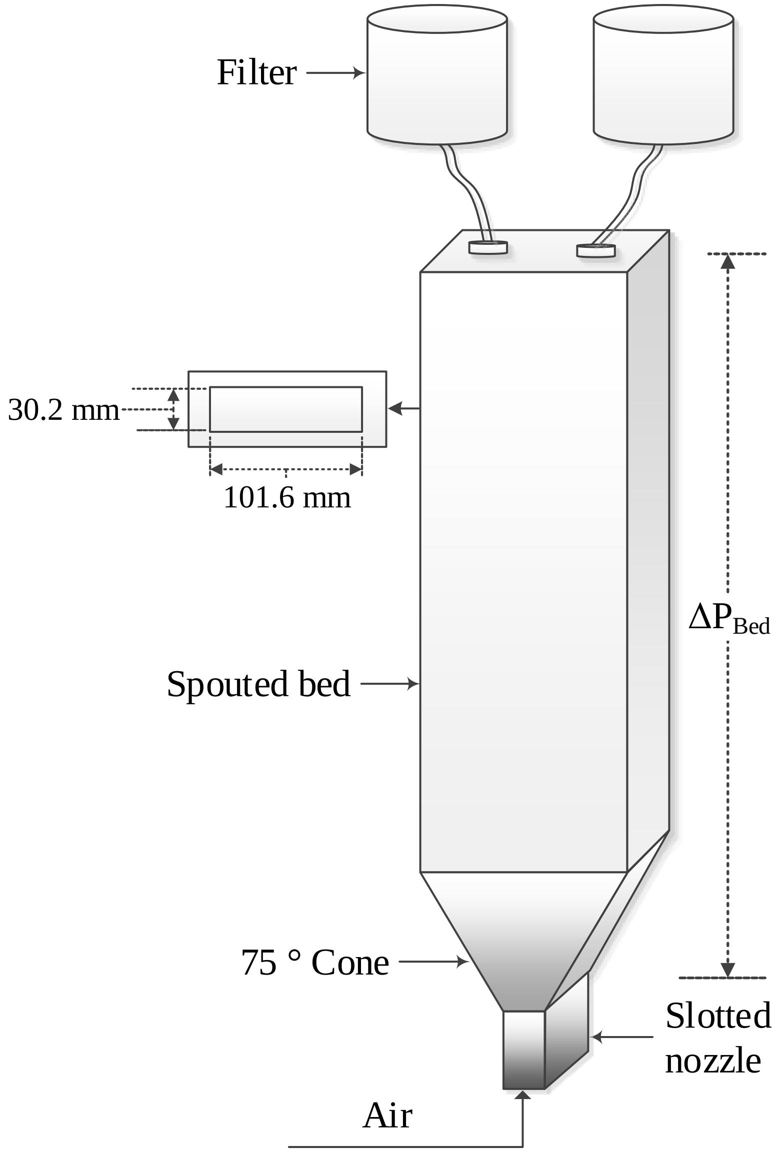

(a)

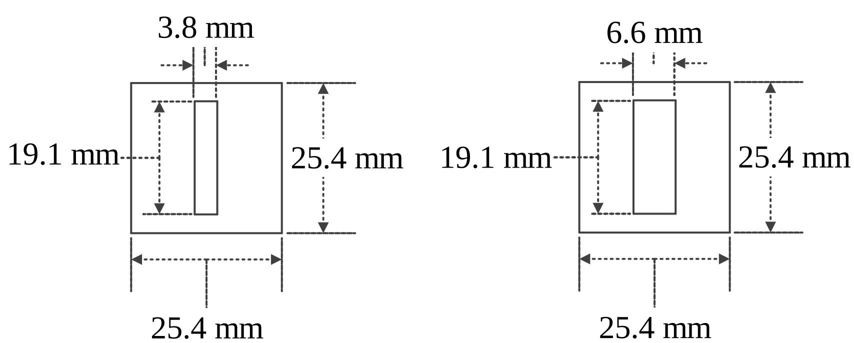

D_{eqn} = 9.6 mm

D_{eqn} = 12.7 mm

(b)

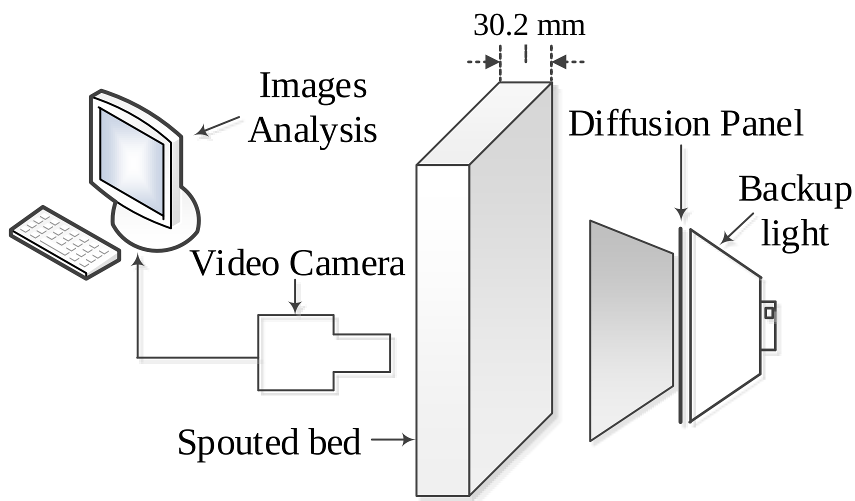

(c)

Figure 1 Schematic diagram of the experimental apparatus: (a) rectangular spouted bed; (b) two different nozzles with detailed dimensions; (c) visualization system.

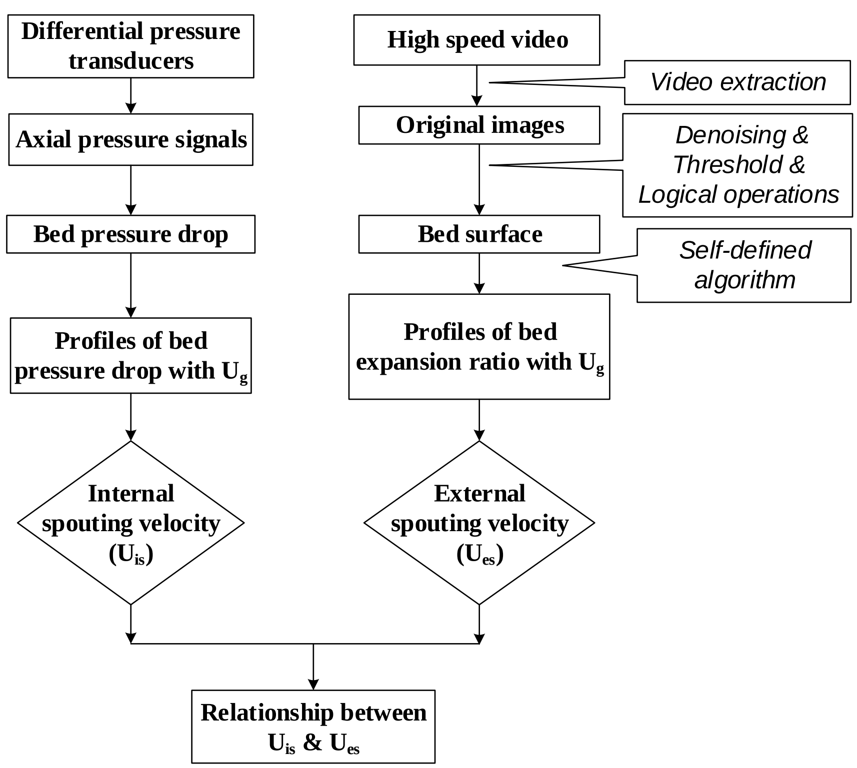

Figure 2 Processing structure of the internal and external spouting velocities.

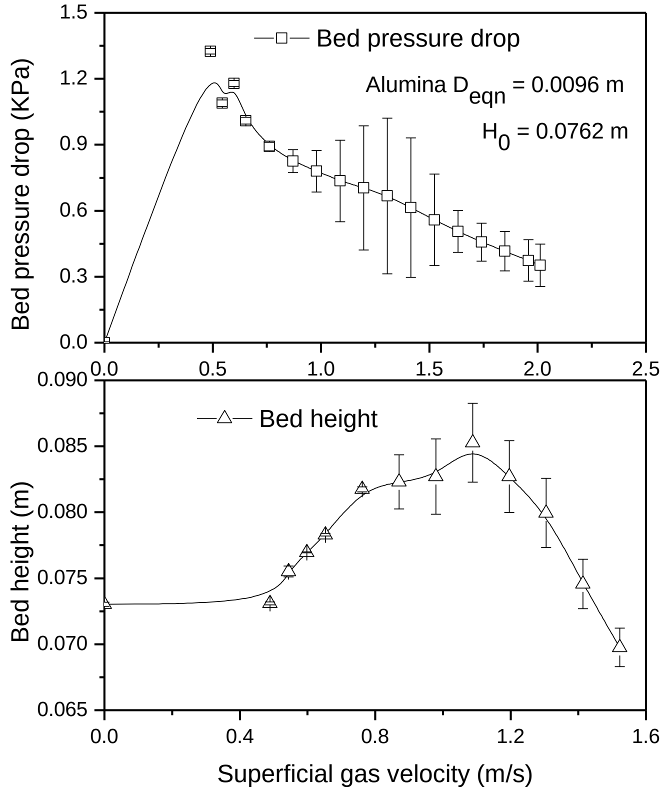

Figure 3 Example of standard deviation of measured bed pressure drop and bed height (Error bars are the ± of one standard deviation).

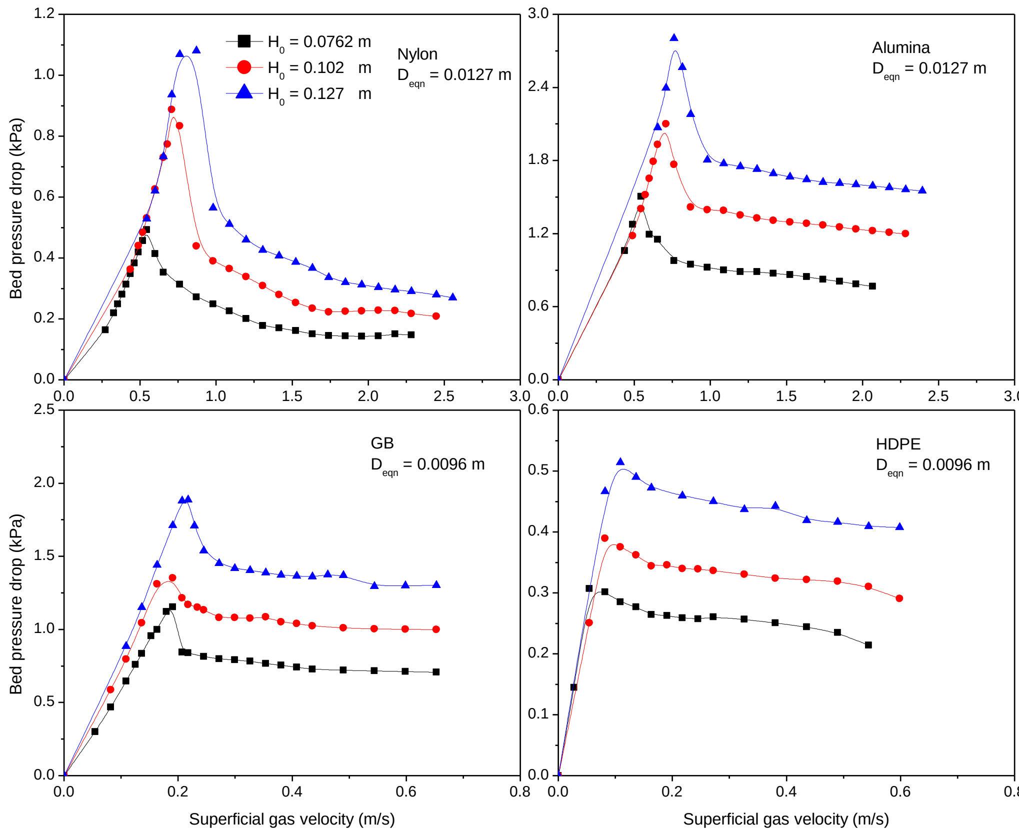

Figure 4 Variation of bed pressure drop with U_g for different kinds of particles.

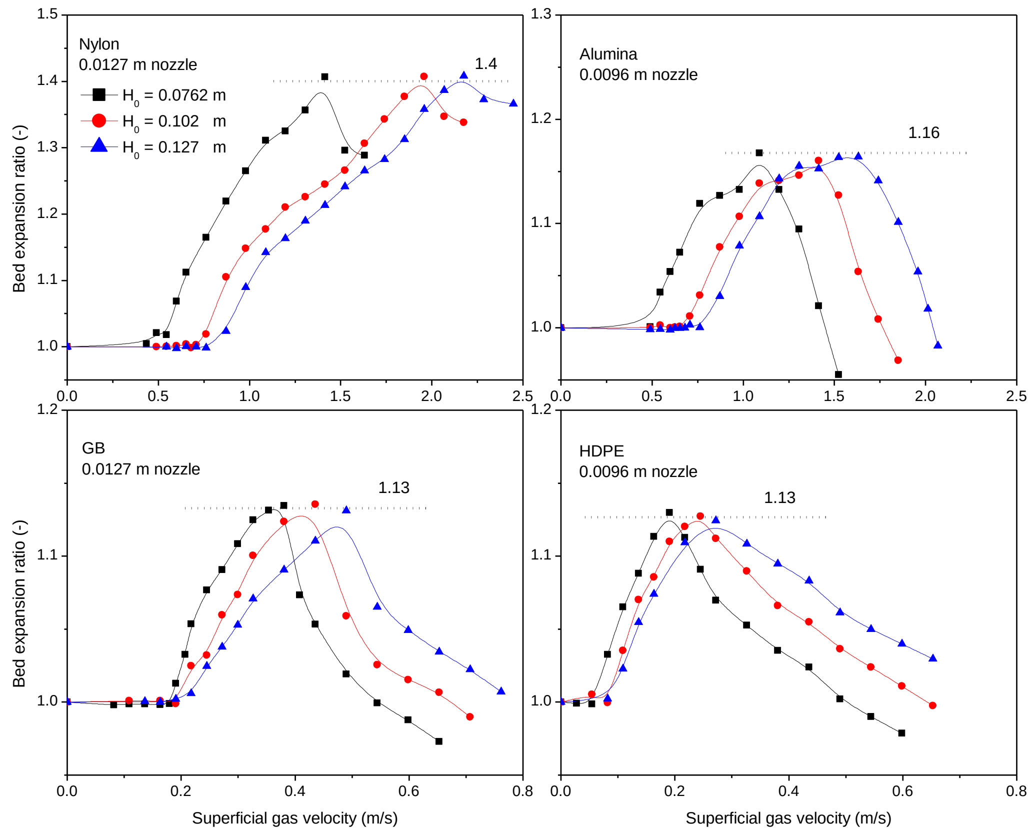

Figure 5 Variation of bed expansion ratio with U_g for different kinds of particles.

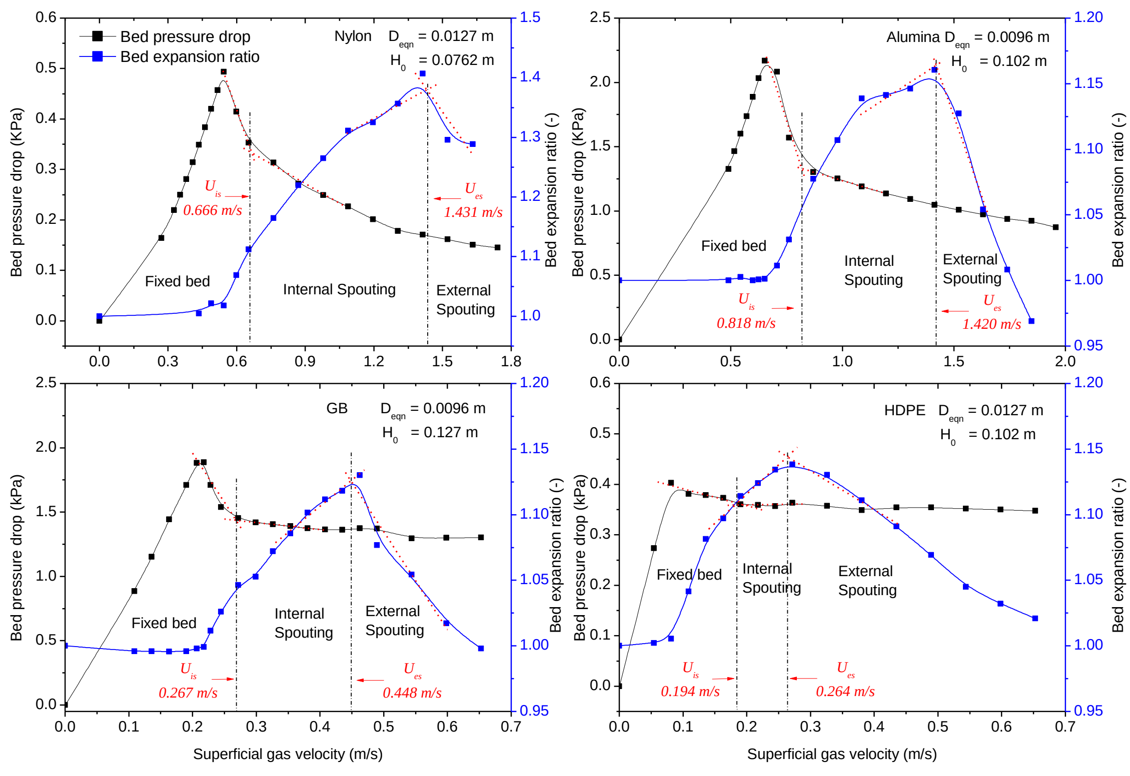

Figure 6 Determination of U_{is} and U_{es} for different kinds of particles.

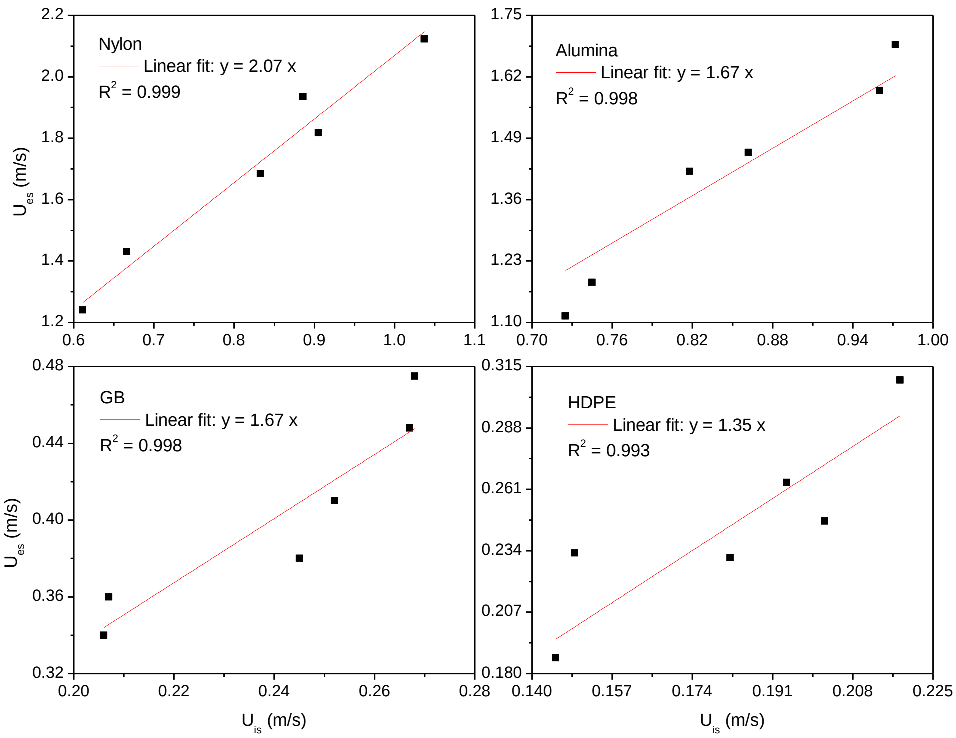

Figure 7 Correlations between U_{is} and U_{es} for the four particle types.

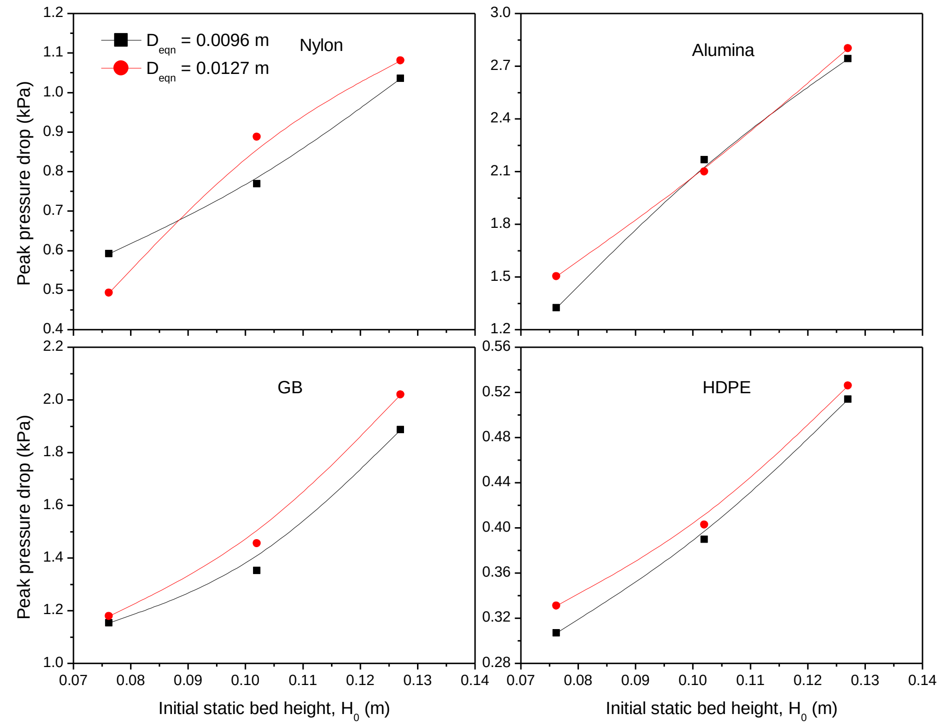

Figure 8 Effect of nozzle size on the peak pressure drop for different kinds of particles.

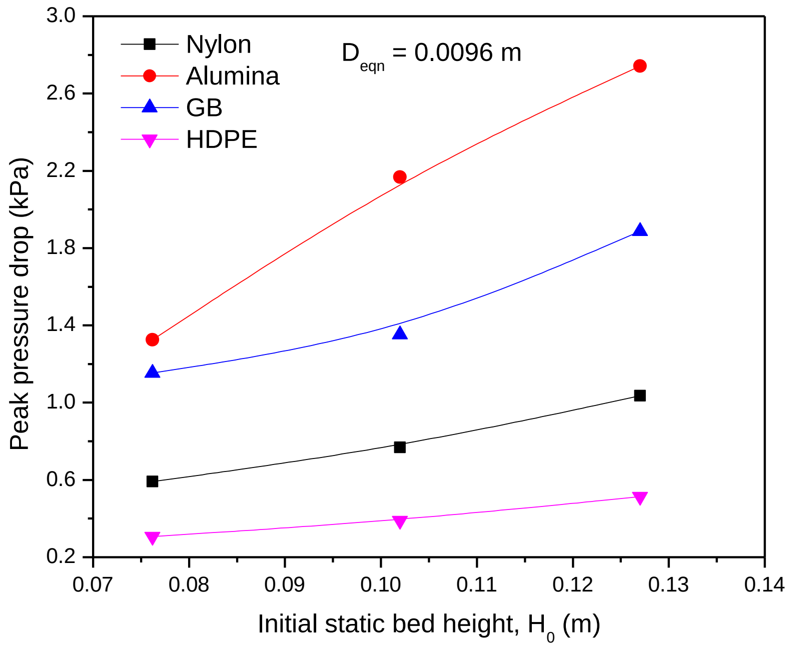

Figure 9 Peak pressure drop for different kinds of particles.

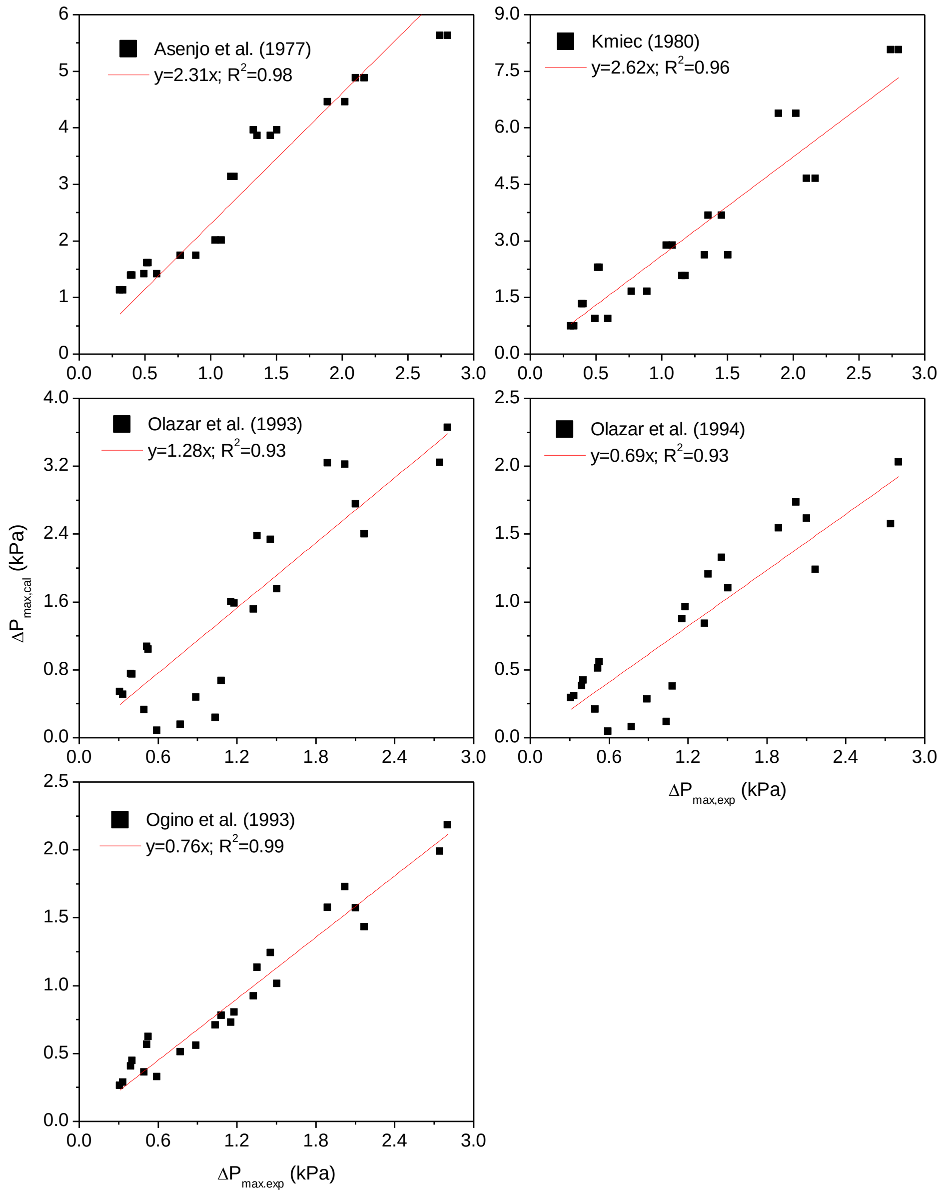

Figure 10 Comparison of experimental peak pressure drop data with calculated data using previous correlations.

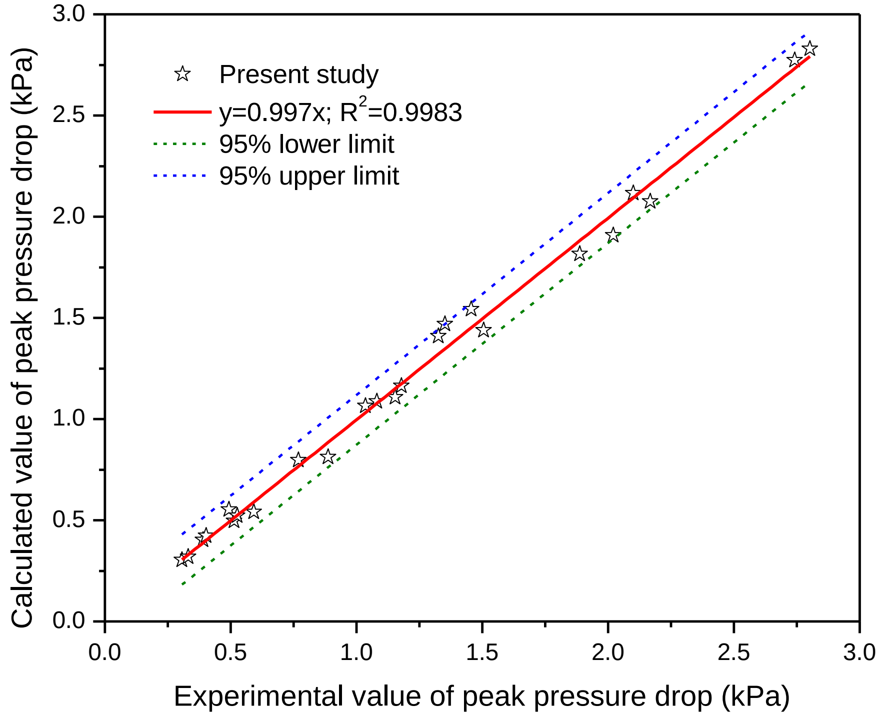

Figure 11 Comparison of experimental peak pressure drop data with calculated data using Eqs. (2) and (3).

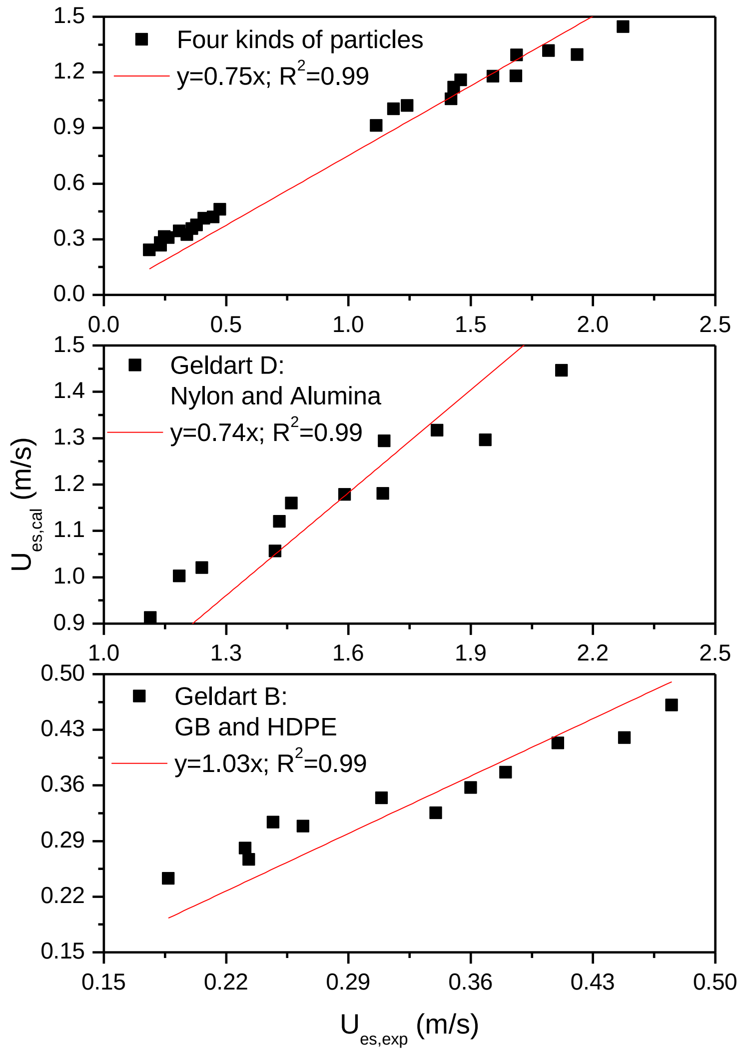

Figure 12 Comparison between experimental and calculated external spouting velocity using Mathur-Gishler equation.

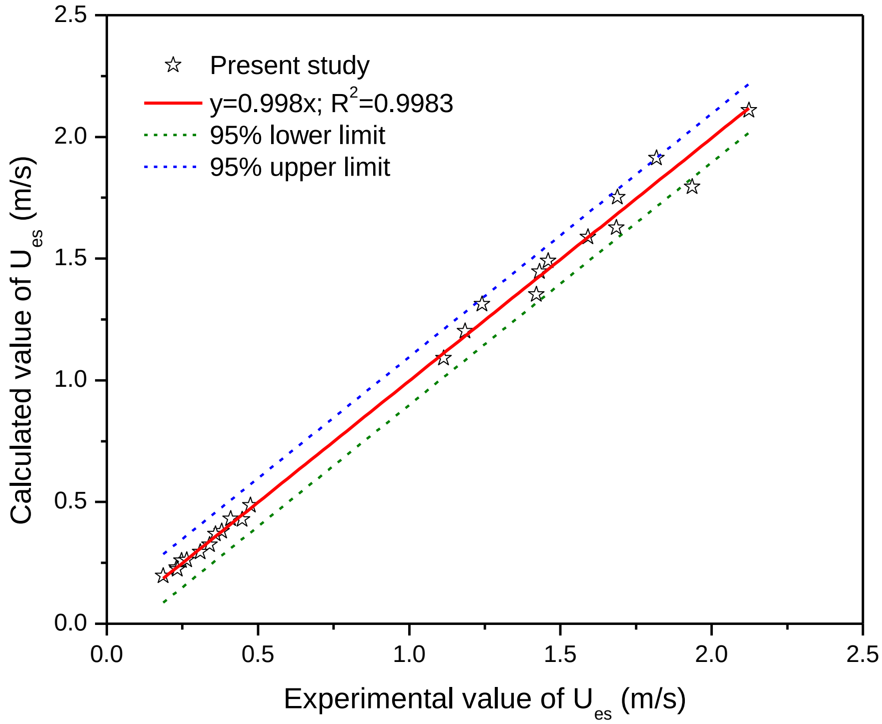

Figure 13 Comparison of experimental U_{es} data with calculated data using Eqs. (6) and (7).

Table 1 Particle properties.

Particles	Sauter mean diameter (μm)	Particle density (kg/m^3)	Minimum fluidization velocity (m/s)	Particle sphericity (-)	Bed void fraction (-)	Bulk density (Fluffed) (kg/m^3)	Geldart Classification
Nylon	3190	1130	1.088	0.95	0.43	650	D
Alumina (solid)	1709	3150	1.101	0.95	0.42	1820	D
Glass beads	713	2300	0.246	0.94	0.38	1440	B
HDPE	871	860	0.174	0.92	0.39	520	B

Table 2 Regime evolution of the different kinds of particles in the current operating condition.

Operating conditions	Regime evolution		
	Static	Internal spouting (Jet development)	External spouting (Fountain formation)
Schematic illustration	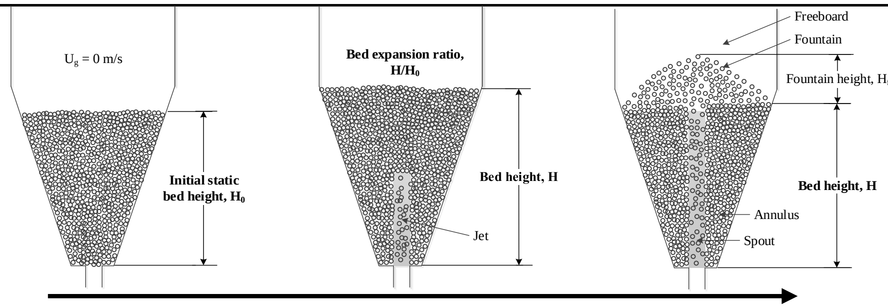 Increasing gas flow rate		
Nylon H_0 = 0.102 m; D_{eqn} = 0.0096 m		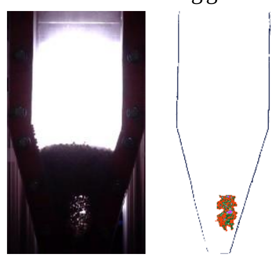	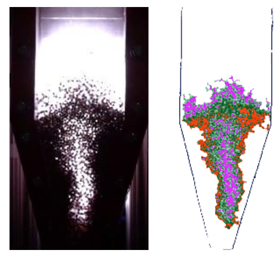
Alumina H_0 = 0.0762 m; D_{eqn} = 0.0096 m		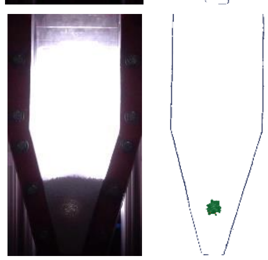	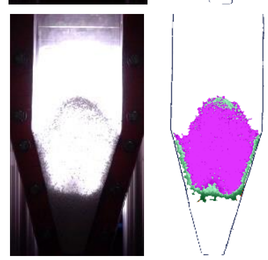
Glass beads H_0 = 0.102 m; D_{eqn} = 0.0127 m			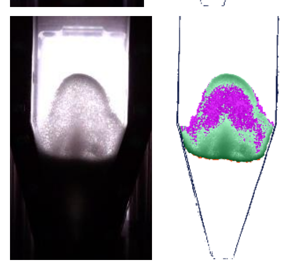
HDPE H_0 = 0.127 m; D_{eqn} = 0.0127 m			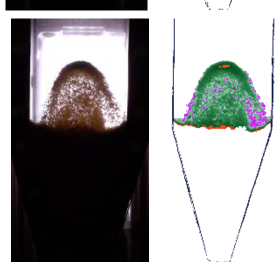

Table 3 U_{is} and U_{es} for the present bed materials.

Particles	Nozzle size, D_{eqn} (m)	Initial static bed height, H_0 (m)	U_{is} (m/s)	U_{es} (m/s)
Nylon	0.0096	0.0762	0.611	1.241
		0.102	0.833	1.685
		0.127	0.905	1.818
	0.0127	0.0762	0.666	1.431
		0.102	0.886	1.936
		0.127	1.037	2.123
Alumina	0.0096	0.0762	0.725	1.114
		0.102	0.818	1.42
		0.127	0.96	1.591
	0.0127	0.0762	0.745	1.185
		0.102	0.862	1.46
		0.127	0.972	1.688
Glass beads	0.0096	0.0762	0.206	0.34
		0.102	0.245	0.38
		0.127	0.267	0.448
	0.0127	0.0762	0.207	0.36
		0.102	0.252	0.41
		0.127	0.268	0.475
HDPE	0.0096	0.0762	0.145	0.187
		0.102	0.182	0.231
		0.127	0.202	0.247
	0.0127	0.0762	0.149	0.233
		0.102	0.194	0.264
		0.127	0.218	0.309

Table 4 Correlations for peak pressure drop in cited literatures.

Authors (Published year)	Correlations	Bed geometry	Note: Slope; R^2 (Applied with the data of the present study)
Gelperin et al.[16] (1961)	$\frac{\Delta P_M}{\rho_b g H_0} = 1 + 0.062\left(\frac{D_c}{D_i}\right)^{2.54}\left(\frac{D_c}{D_i} - 1\right)\left(tan\frac{\theta}{2}\right)^{-0.18}$	Conical	28.65; 0.79
Asenjo et al.[17] (1978)	$\frac{\Delta P_M}{\rho_b g H_0} = 1 + 2.8e^{-0.312H_0/D_c}$	Cylindrical flat-based	2.31; 0.98
Kmieć.[18] (1980)	$\frac{\Delta P_M}{\rho_b g H_0} = 1 + 0.206e^{1.24H_0/D_c}$	Conical	2.62; 0.96
Ogino et al.[19] (1993)	$\frac{\Delta P_M}{\rho_b g H_0} = 1.15\left(\frac{H_0}{D_c}\right)^{1/2}\left(\frac{D_i}{D_c}\right)^{1/3}$	Cylindrical	0.76; 0.99
Rocha et al.[20] (1995)	$\frac{\Delta P_M}{\rho_b g H_0} = 1 + 0.0006\left(\frac{D_c}{D_i}\right)^{5.04}\left(\frac{d_p}{\phi D_c} - 1\right)^{-1.92}$	Slot-rectangular	N/A $\because d_p < D_c$ & $[d_p/(\varphi D_c) - 1] \in (-1, 0)$ $\therefore \nexists [d_p/(\varphi D_c)-1]^{-1.92}$
Mukhlenov and Gorshtein[21] (1965)	$\frac{\Delta P_M}{\Delta P_s} = 1 + 6.65\left(\frac{H_0}{D_i}\right)^{1.2}\left(tan\frac{\theta}{2}\right)^{0.5} Ar^{0.2}$	Conical	369.93; 0.91
Olazar et al.[22] (1993)	$\frac{\Delta P_M}{\Delta P_s} = 1 + 0.116\left(\frac{H_0}{D_i}\right)^{0.5}\left(tan\frac{\theta}{2}\right)^{-0.8} Ar^{0.0125}$	Conical	1.28; 0.93
Olazar et al.[23] (1994)	$\frac{\Delta P_M}{\Delta P_s} = 1 + 0.35\left(\frac{H_0}{D_c}\right)^{0.1}\left(\frac{D_i}{D_c}\right)^{1.1} Ar^{0.1}$	Cylindrical	0.69; 0.93
Monazam et al.[26] (2018)	$\frac{\Delta P_M}{\rho_g U_m^2} = 1.069\left(\frac{H_0}{D_c}\right)^{0.65}\left(\frac{2gH_0(\rho_p - \rho_g)}{\rho_g}\right)^{0.3575}\left(1 + 2.343\left(\frac{U_g}{U_{mf}}\right)^{2.827}\left(\frac{H_0}{D_c}\right)^{-0.843}\left(\frac{2gH_0(\rho_p - \rho_g)}{\rho_g}\right)^{0.297}\right)$	Cylindrical flat-based	7.01; 0.63